AMERICAN SOCIETY FOR MICROBIOLOGY | Molecular and Cellular Biology®

RESEARCH ARTICLE

Coordinated Regulation of Intracellular Fascin Distribution Governs Tumor Microvesicle Release and Invasive Cell Capacity

James W. Clancy,[a] Christopher J. Tricarico,[a] Daniel R. Marous,[a] Crislyn D'Souza-Schorey[a]

[a]Department of Biological Sciences, University of Notre Dame, Notre Dame, Indiana, USA

ABSTRACT Tumor cell invasion is one result of the bidirectional interactions occurring between tumor cells and the surrounding milieu. The ability of tumor cells to invade through the extracellular matrix is in part regulated by the formation of a class of protease-loaded extracellular vesicles, called tumor microvesicles (TMVs), which are released directly from the cell surface. Here we show that the actin bundling protein, fascin, redistributes to the cell periphery in a ternary complex with podocalyxin and ezrin, where it promotes TMV release. The peripheral localization of fascin is prompted by the loss of Rab35 signaling, which in turn unleashes ARF6 activation. The result is a mechanism through which Rab35 and ARF6 cooperatively and simultaneously regulate the distribution and localization of fascin and promote oncogenic signaling, which leads to TMV release while inhibiting invadopodium formation. These studies are clinically significant as fascin-loaded TMVs can be detected in bodily fluids and elevated fascin expression coupled with low Rab35 levels correlates with poor overall survival in some cancers.

KEYWORDS fascin, cell invasion, microvesicles

Invading tumor cells encounter a complex extracellular environment, which requires coordinated and adaptive cellular processes to facilitate migration and invasion (1, 2). Robust cell invasion relies on the ability of tumor cells to readily and interchangeably adopt two distinct phenotypes during motility and invasion: a mesenchymal morphology on rigid matrices, wherein cells are flattened, elongated, and form invadopodia, or an amoeboid morphology on compliant matrices that is characterized by cell rounding, membrane blebbing, and microvesicle shedding (3–6). This regulated shedding of a diverse population of extracellular vesicles by tumor cells has gained traction as a crucial mechanism through which cells reciprocally interact with the extracellular environment (7–9). Among these populations, tumor microvesicles (TMVs) have emerged as critical components of the tumor cell arsenal utilized to degrade extracellular matrix during amoeboid-type cell invasion (6, 10, 11). Furthermore, exosomes released at sites of invadopodium-mediated invasion have been thought to facilitate focal matrix degradation (12). Unlike exosomes, TMVs are actively shed directly into the extracellular space via the outward budding and pinching of the plasma membrane at which time, as we have previously shown, they can be readily detected in peripheral bodily fluids (8, 9, 11, 13, 14). TMV shedding is a highly regulated process with cellular control over macromolecular cargo, fission, and release (8). TMV shedding is at least in part regulated through the activation of the small, Ras-related GTPase, ADP-ribosylation factor 6 (ARF6), through its well-documented roles regulating actomyosin contractility and endosomal membrane recycling, two pathways also regulated by Rab35 (15–17).

Rab35 is a member of the large Rab family of GTPases, with endogenous localization to both the plasma membrane and a pool of endosomal membranes (18). Rab35,

Citation Clancy JW, Tricarico CJ, Marous DR, D'Souza-Schorey C. 2019. Coordinated regulation of intracellular fascin distribution governs tumor microvesicle release and invasive cell capacity. Mol Cell Biol 39:e00264-18. https://doi.org/10.1128/MCB.00264-18.

Address correspondence to Crislyn D'Souza-Schorey, cdsouzas@nd.edu.

Received 22 May 2018
Returned for modification 19 July 2018
Accepted 31 October 2018
Accepted manuscript posted online 5 November 2018
Published 16 January 2019

through its effector proteins, now has known roles in myriad cellular processes, many of which are dysregulated during cancer pathogenesis (17). ARF6 and Rab35 activation is regulated by their interactions with guanine nucleotide exchange factors (GEFs) and GTPase-activating proteins (GAPs). These interactions include instances where effector proteins for one GTPase act as GAPs for the other (17–23), wherein Rab35-mediated regulation is superimposed upon ARF6 activity and regulation with potential impacts on a wide array of intracellular processes.

Despite a growing body of literature, the mechanisms and regulation of TMV biogenesis are not fully understood and require further investigation. Here, we identify a mechanism through which antagonistic GTPase signaling is coupled to intracellular fascin localization to regulate the shedding of invasive TMVs. Rab35 activation suppresses TMV shedding from invasive tumor cells by modulating ARF6 activity and, further, regulating intracellular fascin localization. Depletion of endogenous Rab35 leads to increased levels of ARF6-GTP, a primarily peripheral redistribution of fascin where it resides in a ternary complex with ezrin and podocalyxin, and a dramatic increase in TMV shedding during amoeboid cell invasion. These results are particularly relevant in light of several previous reports that fascin is a direct downstream effector of Rab35, where it governs Rab35-regulated actin bundling, and its inhibition by migrastatin analogues successfully blocks tumor cell invasion and metastasis *in vivo* (16, 24). Furthermore, as we describe below, elevated fascin expression correlates with decreased overall survival, highlighting the need for increased understanding of its role in tumor progression.

RESULTS

Rab35 signaling functions to modulate tumor microvesicle shedding. In light of multiple literature reports outlining roles for Rab35 and ARF6 in regulating endosomal recycling (18), together with previously identified pathways through which ARF6 activation governs the release of TMVs from the surface of multiple tumor cell types (6, 13), we sought to examine the impact of Rab35 activation on the shedding of invasive TMVs. Expression of the constitutively active GTP-bound mutant of Rab35, Rab35-Q67L, in the melanoma cell line, LOX, resulted in significantly decreased TMV shedding as measured by nanoparticle tracking analysis (NTA) (Fig. 1A and B) and Western blotting (Fig. 1C). Conversely, Rab35 inactivation through expression of the GDP-bound, dominant-negative Rab35-S22N increased the release of TMVs (Fig. 1A to C). These results, which suggest that under normal conditions, elevated Rab35 activity suppresses TMV shedding, led us to examine the effect of depleting endogenous Rab35 on TMV production. To this end, we made use of clustered, regularly interspaced, short palindromic repeat (CRISPR) Cas9 technology to disrupt the endogenous Rab35 genomic locus in multiple cell lines, followed by either clonal or pharmacological selection. Expansion resulted in the generation of LOX, A375-MA2, and A375-P melanoma cells with reduced or depleted levels of Rab35 (Fig. 1D and E). Examination of the culture supernatant from LOX^{Rab35KO} clonal cells and lines generated by puromycin selection revealed a striking increase in the release of TMVs when examined by NTA (Fig. 1F and G) or immunofluorescence (Fig. 1H). In addition to melanoma, we have previously identified a similar population of ARF6-positive, invasive TMVs in the ascites of ovarian cancer patients (11). Given this, we also examined the impact of Rab35 signaling on TMV release from the high-grade serous ovarian cancer cell line OvCar3 and confirmed that modulation of Rab35 signaling or depletion of Rab35 resulted in increased TMV shedding (Fig. 1I to K).

Loss of endogenous Rab35 enhances amoeboid-like cell invasion. We examined the effects of Rab35 depletion on both TMV shedding and invasion using our *in vitro* cell invasion assay utilizing compliant matrices which drives tumor cells to adopt amoeboid morphologies during invasion (6). Coupled to this conversion, amoeboid cells readily shed TMVs and exhibit directed movement as cells form "trails" of degraded matrix, here referred to as "amoeboid invasion," which allows quantification of the distance invaded (6, 11). LOX^{Rab35KO} cells released significantly more TMVs than

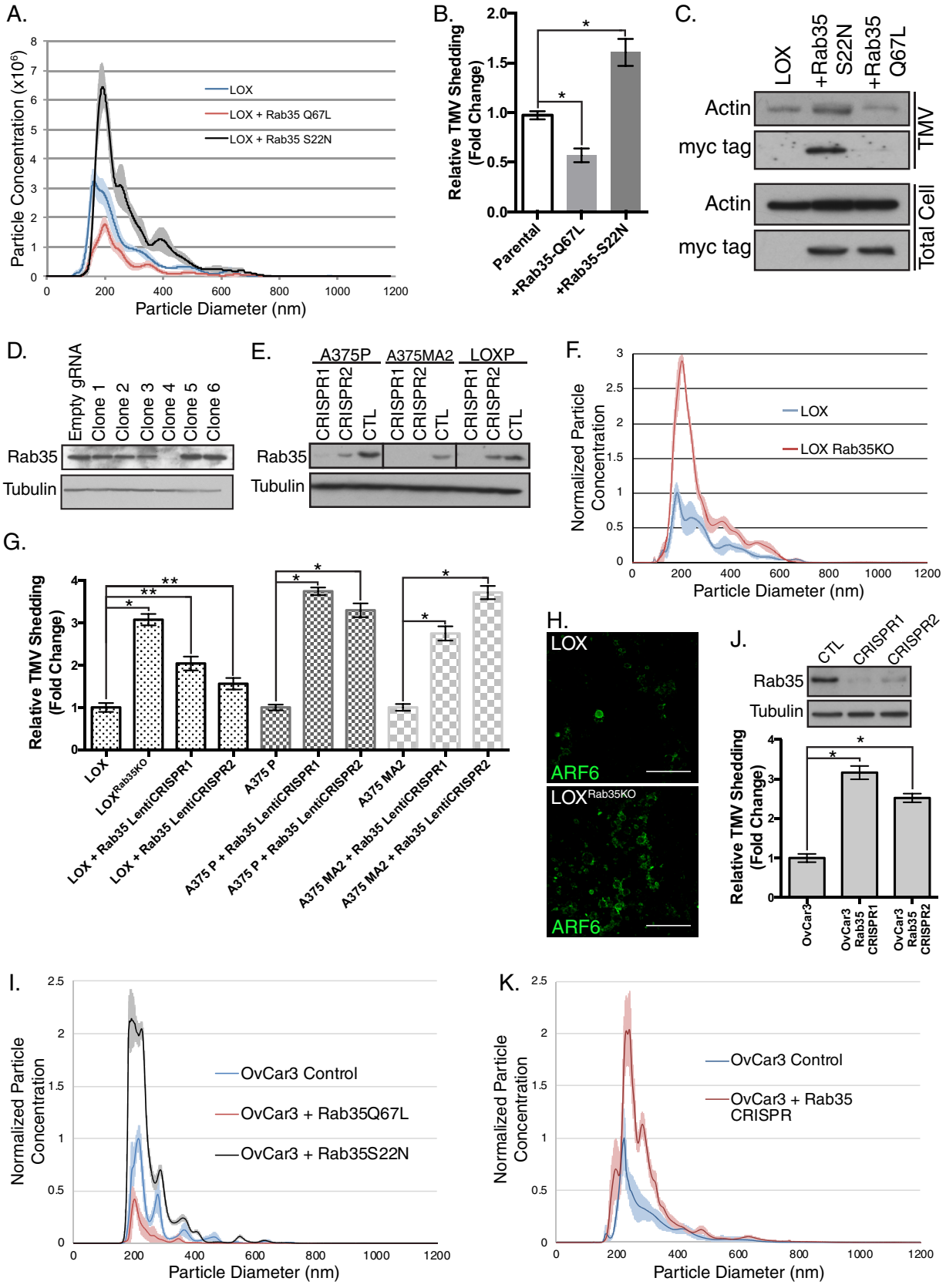

FIG 1 Rab35 activation alters TMV shedding. (A) TMVs from an equal number of control LOX cells, along with cells expressing Rab35-Q67L or Rab35-S22N, were isolated and analyzed by NTA. Data are presented as means ± the standard errors of the mean (SEM) of replicate measures at each particle diameter. (B) TMV concentrations in conditioned media from cells expressing constitutively active (Q67L) and dominant-negative

(Continued on next page)

their parental counterparts during amoeboid invasion (Fig. 2A, arrows) with a concomitant increase in amoeboid invasive capacity as shown with the significantly longer trails of degraded matrix left in their wake (Fig. 2A and B). This increase in amoeboid invasive capacity can, in line with previous reports, be blocked through the expression of dominant-negative ARF6 (ARF6-T27N) (6) (Fig. 2B). As we have previously shown, the inclusion of proteolytically active MT1-MMP is critical to TMV functionality during tumor cell invasion, particularly in complete collagen matrices where, under physiological conditions, proteolysis is required to open and expand matrix pores to allow for invasion (11, 25, 26). Consistent with the increase in amoeboid invasion, Western blot examination of isolated TMVs released from LOX^{Rab35KO} cells revealed that they retain known TMV cargoes, including MT1-MMP (Fig. 2C), which suggests that Rab35 has no effect on the trafficking of the metalloprotease to TMVs. In addition to direct proteolysis of the extracellular matrix, TMVs can alter the behavior of neighboring cells. To examine the impact of Rab35 knockout on recipient cell behavior, we incubated parental LOX cells with an equal number of TMVs isolated from LOX^{Rab35KO} cells or the parental line as an orthotopic control. Treatment with isolated TMVs resulted in an increase in matrix degradative and invasive capacity (Fig. 2D to G), suggesting this stimulatory effect is TMV specific and not modulated by the loss of Rab35. Furthermore, these results highlight the multifaceted roles for TMVs during tumor cell invasion, where TMVs can directly act to degrade the extracellular matrix, and drive increased recipient cell invasion. Taken together, these findings demonstrate that the loss of Rab35 leads to a robust increase in the shedding of functional protease-loaded TMVs and increased amoeboid invasive capacity.

Rab35 knockout unleashes ARF6-driven TMV shedding. Phenotypic similarities among LOX^{Rab35KO} and LOX$^{ARF6\text{-}GTP}$ cells, both of which readily adopt amoeboid morphologies and increase TMV shedding (13), along with the reciprocal relationship between Rab35 and ARF6 (18, 20), led us to examine the activation state of ARF6 upon loss of Rab35. Loss of Rab35 leads to an increase in active ARF6-GTP relative to the parental cell line (Fig. 3A). Furthermore, amoeboid invasion (Fig. 3B, quantified in Fig. 2B) and TMV shedding (assessed by NTA analysis) (Fig. 3C to E) is blocked by transient expression of the dominant-negative variant of ARF6, ARF6-T27N in LOX^{Rab35KO} cells, suggesting that an ARF6-dependent TMV shedding mechanism is unleashed upon depletion of Rab35.

To confirm that Rab35 knockdown facilitates ARF6-GTP-mediated TMV shedding, we examined pathways signaling downstream of ARF6 activation (6, 13). Consistent with increased levels of ARF6-GTP and in line with previous reports linking the loss of Rab35 expression to activation of ARF6 and adoption of hallmarks of malignant progression (27), Rab35 knockdown results in a striking increase in phosphorylated ERK1/2 detected by Western blotting (Fig. 3F and G). Subsequent treatment of control or LOX^{Rab35KO} cells with the small molecule inhibitor of ERK activation U-0126 resulted in both a significant decrease in amoeboid cell invasion, as measured by distance invaded and TMV shedding quantified by NTA (Fig. 3H to J). Similar results were obtained by

FIG 1 Legend (Continued)
(S22N) Rab35 were examined relative to the control. Data are presented as means ± the SEM (*, $P < 0.001$). (C) LOX melanoma cells were transfected with constitutively active myc–Rab35-Q67L or dominant-negative myc–Rab35-S22N, and the impact on TMV shedding was examined by Western blotting. (D) Clonal cell lines generated after the expression of Cas9 with guide RNA targeting Rab35 were lysed, and Rab35 protein levels were examined by Western blotting. (E) A375-P, A375-MA2, and LOX cells were infected with Cas9/Rab35gRNA lentivirus to deplete endogenous Rab35. After pharmacological selection, Rab35 levels were examined by Western blotting. (F) Isolated TMVs released from equal numbers of LOX or LOX^{Rab35KO} cells were quantified by NTA. Data are presented as means ± the SEM of replicate measures at each particle diameter. (G) TMV concentrations in conditioned media conditioned by cells described for panel E were determined by NTA. Data are presented as means ± the SEM (*, $P < 0.001$; **, $P < 0.005$). (H) TMVs isolated from equal numbers of LOX or LOX^{Rab35KO} cells were overlaid onto poly-L-lysine-coated coverslips. After 16 h, the TMV were fixed, stained as indicated and analyzed by confocal microscopy. Scale bars, 10 μm. (I) OvCar3 cells were infected with retrovirus to express constitutively active Rab35-Q67L, dominant-negative Rab35-S22N, or empty vector (Control). At 60 h postinfection, the cells were switched to EV-free media and cultured for an additional 24 h. TMVs were then isolated from the media and examined by NTA. (J) OvCar3 cells were infected with Cas9/Rab35gRNA lentivirus to deplete endogenous Rab35. The Rab35 levels were then examined by Western blotting, and TMV concentrations in conditioned media were measured by NTA. Data are presented as means ± the SEM (*, $P < 0.001$). (K) OvCar3 cells were infected with lentiCRISPRv2-Rab35 virus, and TMVs were examined as described previously (D). Data are presented as means ± the SEM of replicate measures at each particle diameter.

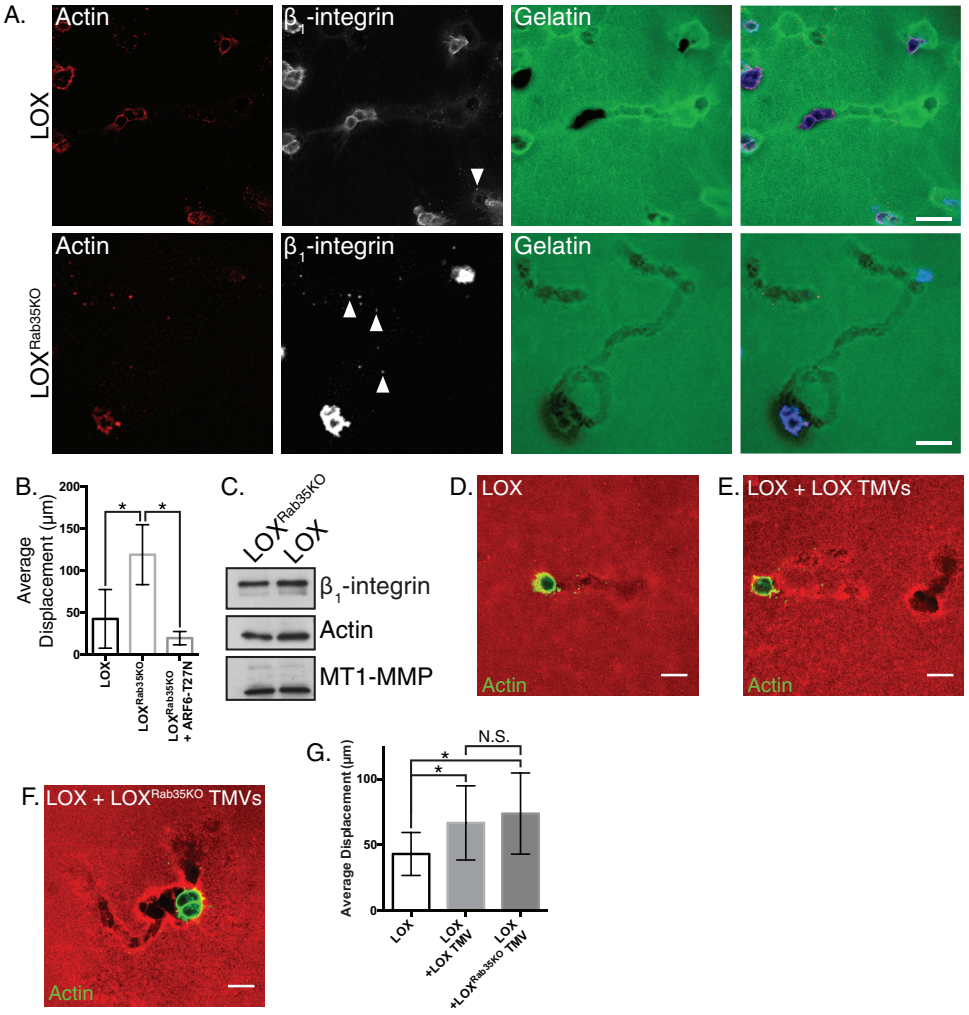

FIG 2 Rab35 knockout facilitates amoeboid cell invasion. (A) LOX or LOX^{Rab35KO} cells were plated in an *in vitro* amoeboid cell invasion assay and allowed to invade for 24 h. Invasive cells were fixed, stained as indicated, and examined by confocal microscopy in order to quantify changes in invasive potential. Scale bars, 25 μm. (B) The average displacement of LOX, LOX^{Rab35KO}, and LOX^{Rab35KO} cells expressing ARF6-T27N was calculated after 8 h of invasion into compliant matrix. Data are presented as means ± the standard deviations (SD; *, $P < 0.05$). (C) Equal amounts of protein contained in lysates generated from TMVs isolated from LOX or LOX^{Rab35KO} cells were separated by SDS-PAGE, and the cargo content was examined as indicated by Western blotting. (D to F) Parental LOX cells alone (D) or pretreated with TMVs isolated from LOX cells (E) or LOX^{Rab35KO} cells (F) were plated in an amoeboid invasion assay. After 8 h of invasion, the cells were fixed, and the actin cytoskeleton was stained and imaged. Scale bars, 20 μm. (G) The average displacement per field of cells described for panels D to F was calculated after 8 h of invasion into compliant matrix. Data are presented as means ± the SD (*, $P < 0.05$; N.S., not statistically significant).

blocking myosin light chain (MLC) activation (Fig. 4A to C) or ROCK activity (Fig. 4D to F), using ML-7 and Y-27632, respectively, both of which resulted in a robust block in TMV release from LOX^{Rab35KO} cells. Notably, even with the robust activation of proinvasive signaling cascades and phenotypic changes, we found a slight reduction in the pAKT levels (Fig. 4G) and proliferative capacity (Fig. 4H), suggesting pleiotropic effects result from Rab35 signaling pre- and post-malignant transformation (28). Taken together, these results confirm that the loss of Rab35 facilitates TMV shedding by uncoupling parallel ARF6-mediated signaling from antagonistic repression by active Rab35-GTP.

Loss of Rab35 alters fascin localization to enable TMV shedding. In flat cells with mesenchymal cell-type morphologies, elevated levels of ARF6-GTP result in increased matrix degradation and invasion at the ventral surface (29, 30) owing to the formation

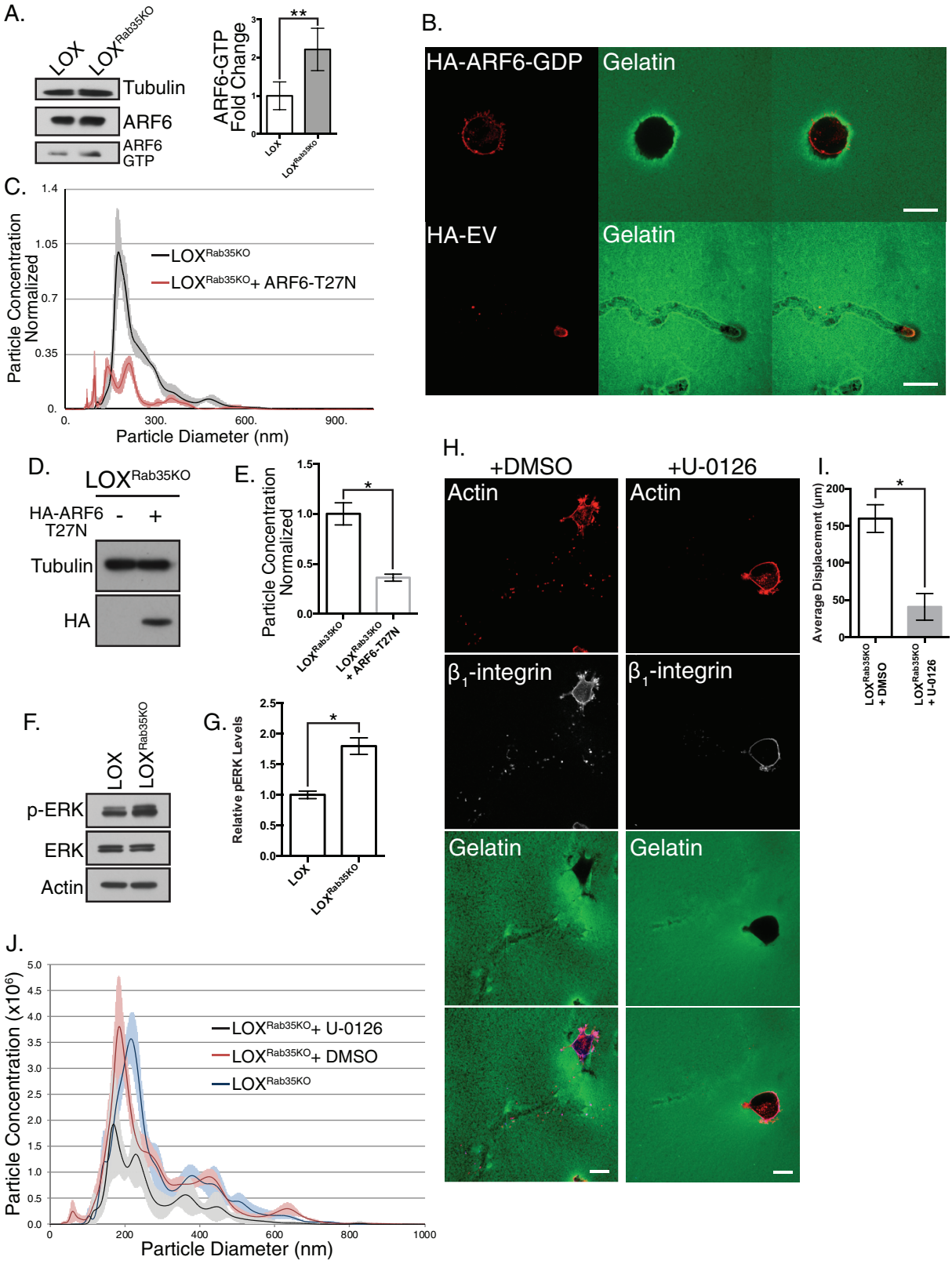

FIG 3 Rab35 knockout uncouples ARF6-regulated TMV shedding. (A) Control and LOX^{Rab35KO} cells were lysed and subjected to MT2-based GTP-specific pulldown as described in Materials and Methods. Loss of Rab35 leads to increased levels of ARF6-GTP. Data are presented as means ± the SD (*, $P < 0.035$). (B) Expression of dominant-negative ARF6-T27N in LOX^{Rab35KO} cells in an amoeboid cell invasion assay blocks invasion placing ARF6 activity downstream of Rab35. Scale bars, 25 μm (top panel) or 75 μm (lower panel). The quantification is shown in Fig. 2B. (C) LOX^{Rab35KO} cells were infected with retrovirus containing HA-ARF6-T27N, and the TMV levels were measured in conditioned media by nanoparticle tracking. (D) The transduction efficiency of HA-ARF6-T27N retrovirus was determined by Western blotting for the HA tag. (E) Particle

(Continued on next page)

of protease-rich membrane protrusions known as invadopodia (31). ARF6 supports invadopodium biogenesis in part by facilitating the redistribution of invadopodium components, such as cortactin, from the cytoplasm to sites of invadopodium formation (30). Since fascin is both a known component of invadopodia and a direct effector of Rab35, it is possible that an ARF6- and Rab35-regulated pathway recruits fascin to invadopodia (16, 32). Fascin, like actin, has a distinct punctate localization in parental cells (Fig. 5A), where it will colocalize with the invadopodium marker cortactin at the adherent cell surface (Fig. 5B). Further, in addition to its pericellular distribution, puncta of constitutively active Rab35-Q67L are found, along with the invadopodium components fascin and cortactin, at sites where the degradation of the fluorescent matrix results in dark spots in the fluorescent field (Fig. 5C, arrowheads). Dominant inhibition of ARF6 blocks the recruitment of fascin from intracellular compartments to invadopodia with a concomitant loss of invasion and matrix degradation (Fig. 5D). Further, dominant inhibition of Rab35 by Rab35-S22N prevents its association with cortactin and fascin and consequently blocks invadopodium-mediated matrix degradation (Fig. 5E and F), with >90% of cells expressing Rab35-S22N exhibiting this phenotype. In line with these findings, the loss of Rab35, while it results in increased levels of ARF6-GTP, resulted in a near total loss of invadopodium-mediated matrix degradation (Fig. 5G).

Examination of fascin localization in LOX^{Rab35KO} cells revealed that in mesenchymal cells the punctate intracellular distribution of fascin is lost upon Rab35 depletion (Fig. 5H). Instead, as with Rab35-S22N, there is an even more prominent redistribution of fascin to the peripheral, juxtamembrane region. When we examined the effect of transient reintroduction of wild-type Rab35 in LOX^{Rab35KO} cells, we found it was sufficient to restore invadopodium-mediated matrix degradation (Fig. 5I).

Notably, however, on compliant matrices when cells adopt an amoeboid morphology, fascin enrichment could be identified at the necks of nascent TMVs in both LOX and LOX^{Rab35KO} cells (Fig. 6A, arrowheads), areas that contain a similar enrichment of p-MLC (13), and this is consistent with the need for actomyosin contractile machinery in TMV pinching. Thus, antagonistic ARF6 and Rab35 signaling can dictate the intracellular fascin distribution to distinct invasive structures and ultimately the overall mode of invasion. In addition, Rab35, through this relationship with ARF6, regulates activation of the requisite contractile machinery needed for TMV shedding. Taken together, these results underscore the importance of the interaction between Rab35 and the actin bundling protein fascin as an additional albeit unexplored mechanism through which it may regulate TMV shedding (16).

Fascin resides in a peripheral complex with ezrin and podocalyxin in the absence of Rab35. The striking redistribution of fascin in LOX^{Rab35KO} cells led us to examine whether fascin's actin binding activity was facilitating the increase in TMV shedding with Rab35 depletion. To this end, we quantified TMV release in the presence of the small molecule inhibitor FascinG2, which blocks the binding of fascin to actin filaments, reduces tumor cell invasion *in vitro*, and reduces tumor cell metastasis *in vivo* (33). FascinG2 treatment significantly reduced TMV shedding compared to vehicle control in parental LOX and LOX^{Rab35KO} cells (Fig. 6B). In addition to actin, several other fascin binding partners have been identified, including ezrin, a member of the ERM family of proteins linking integral plasma membrane proteins to the cortical actin cytoskeleton. Binding between ezrin and fascin is facilitated by phosphorylation of ezrin at threonine 567 (p-ezrin), a phosphorylation site which is a downstream target of active Rho/ROCK signaling (34, 35). Although Western blotting revealed no significant

FIG 3 Legend (Continued)
concentrations, as measured by NTA, in conditioned media of HA-ARF6-T27N-infected cells. Data are presented as means ± the SEM (*, $P < 0.01$). (F) Lysates from and LOX^{Rab35KO} cells were separated by SDS-PAGE, and the levels of total and phosphorylated ERK were examined by Western blotting. (G) LOX^{Rab35KO} cells show sustained and elevated levels of active ERK. *, $P < 0.01$. (H) LOX^{Rab35KO} cells were treated with the small molecule ERK inhibitor U-0126 or vehicle control during amoeboid cell invasion. Scale bars, 25 μm. (I) The average displacement of the cells described for panel H was calculated after 8 h of invasion into compliant matrix. Data are presented as means ± the SD (*, $P < 0.001$). (J) Nanoparticle tracking analysis of conditioned media from untreated, vehicle control, or U-0126 treated LOX^{Rab35KO} cells. Data are presented as means ± the SEM for each particle diameter.

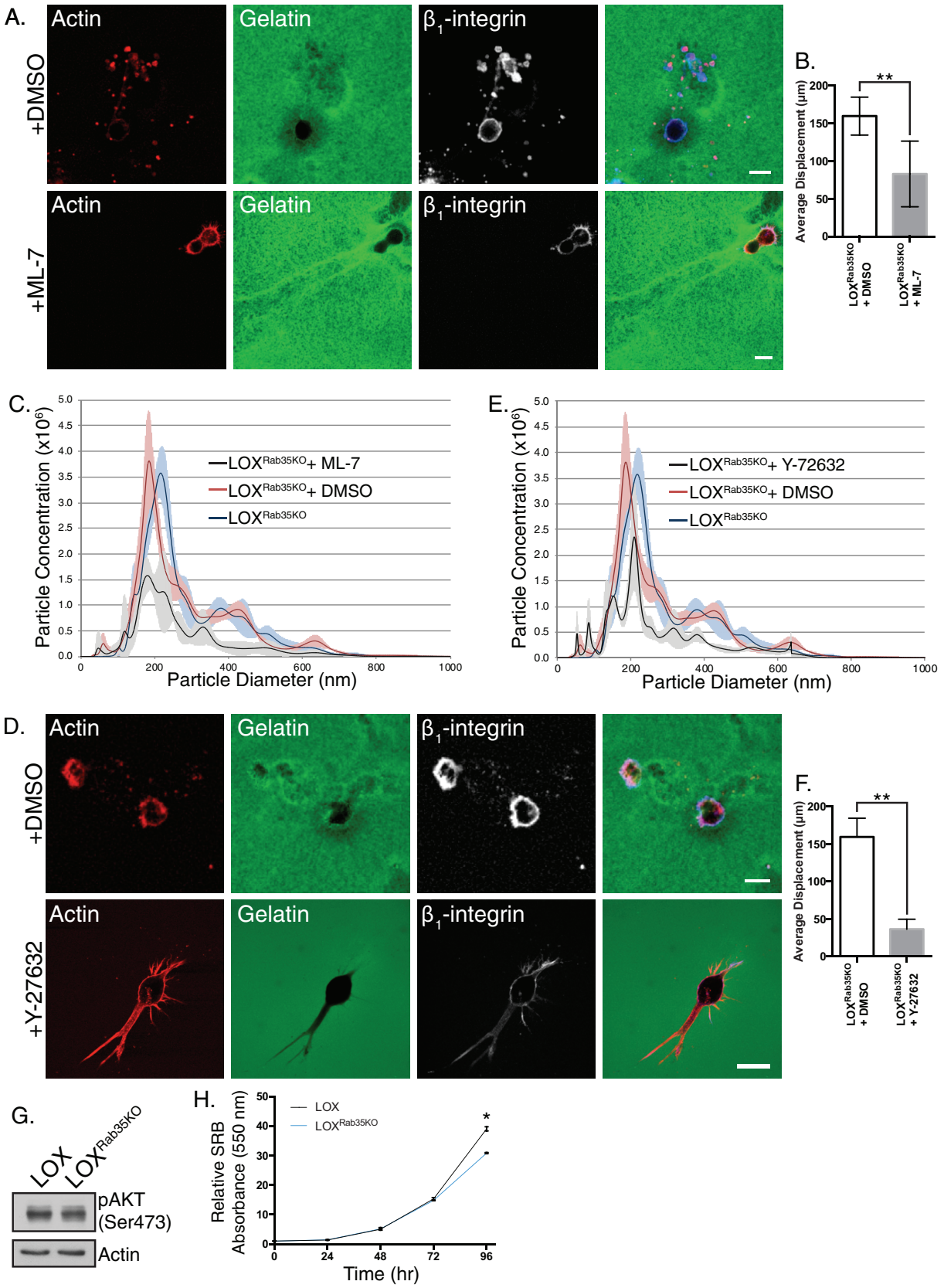

FIG 4 Rab35-regulated TMV shedding requires contractile machinery. (A) LOX^{Rab35KO} cells were treated with the small molecule inhibitor ML-7 or vehicle control during amoeboid cell invasion. Scale bars, 25 μm. (B) The average displacement of cells described for panel A was calculated after 8 h of amoeboid invasion. Data are presented as means $\pm$ the SD (*, $P < 0.001$). (C) Nanoparticle tracking analysis of conditioned media from

(Continued on next page)

difference in p-ezrin levels with a loss of Rab35 (Fig. 6C), immunofluorescence localization showed a more prominent labeling at the cell periphery relative to parental cells (Fig. 6D). Treatment with the small molecule inhibitor of ezrin bioactivity, NSC668394, effectively reduced TMV shedding in LOX and LOX^{Rab35KO} cells (Fig. 6E). In addition to interacting with fascin, p-ezrin is known to bind the type 1 transmembrane glycoprotein, podocalyxin (PODXL), which is itself enriched at the plasma membrane upon Rab35 knockdown (36, 37), suggesting a possible mechanism for the peripheral redistribution of fascin. We examined the interactions between fascin, ezrin, and podocalyxin by immunoprecipitating endogenous ezrin from control and LOX^{Rab35KO} cells. Western blot analysis of precipitated proteins reveals increased levels of both fascin and podocalyxin coprecipitating with ezrin in LOX^{Rab35KO} cells (Fig. 6F and G). In addition, Western blot analysis of lysates generated from equal numbers of TMVs shed from parental or knockout cells showed that while fascin remains TMV cargo upon Rab35 knockout, the amount of fascin per vesicle is decreased (Fig. 6H).

Consistent with fascin expression having been characterized in many carcinomas, including those of the breast, prostate, and ovaries (38), we have localized fascin to the necks of budding TMVs in cell lines of multiple tumor types (Fig. 7A and B). Furthermore, we have previously identified and isolated invasive TMVs from the ascites of ovarian cancer patients (11). We here show that these TMVs also contain fascin and, as previously reported, ARF6, whereas they lack HE-4, which is readily detected in the unfractionated ascites (Fig. 7C). While fully annotated data sets for melanoma are much smaller than other cancer types, interrogation of publicly available expression data from ovarian cancer reveals that elevated fascin expression does not strongly correlate with poor overall survival or progression free survival (Fig. 7D and E). However, when coupled to low expression of Rab35, a negative correlation emerges in both overall survival and progression free survival (Fig. 7F and G). Based on the studies described here, our working model suggests that the loss of Rab35 results in a block in fascin recruitment to invadopodia from Rab35-regulated endomembrane structures. Instead, fascin remains trapped at the cell surface, where it is bound in a complex with ezrin and PODXL and is readily available to facilitate TMV shedding and amoeboid cell invasion (Fig. 8).

DISCUSSION

The findings presented in this study demonstrate that the cellular localization of the actin bundling protein, fascin, is dictated by a balance in the activities of the small GTPases ARF6 and Rab35. This in turn regulates the formation of particular invasive structures, in line with invasive plasticity. Amoeboid-like invading tumor cells maintain dynamic plasma membranes, as multiple protruding blebs form and are subsequently released or retracted. We have previously reported the specific enrichment of phosphorylated MLC at the necks of what appear to be nascent TMVs (13). We propose that the antagonistic relationship between Rab35 and ARF6 represents a regulatory mechanism coupling focal actomyosin contractility and the recruitment of critical components of the invasive machinery, including fascin, to sites of TMV or invadopodium biogenesis. Tight regulation of the intrinsic contractile machinery is of heightened importance since small molecule inhibitors of fascin and ezrin have shown significant promise in their ability to block cell invasion and metastasis *in vivo* (24, 33, 39).

That the loss of antagonistic Rab35 signaling promotes the release of invasive TMVs further manifests when these cells are cultured in the presence of either rigid or compliant extracellular matrices. Tumor cells, in the presence of compliant matrices,

FIG 4 Legend (Continued)
untreated, vehicle control, or ML-7-treated LOX^{Rab35KO} cells. Data are presented as means ± the SEM for each particle diameter. (D) LOX^{Rab35KO} cells were treated with the ROCK inhibitor Y-27632 or vehicle control during amoeboid cell invasion. Scale bars, 25 μm. (E) Nanoparticle tracking analysis of conditioned media from untreated, vehicle control, or Y-27632-treated LOX^{Rab35KO} cells. Data are presented as means ± the SEM at each particle diameter. (F) The average displacement of cells described for panel D was calculated after 8 h of amoeboid invasion. Data are presented as means ± the SD (*, $P < 0.001$). (G) The levels of phospho-AKT (Ser-473) were measured in LOX and LOX^{Rab35KO} cells by Western blotting. (H) Proliferation was quantified in LOX and LOX^{Rab35KO} cells using a sulforhodamine B assay. Data are presented as means ± the SD (*, $P < 0.02$).

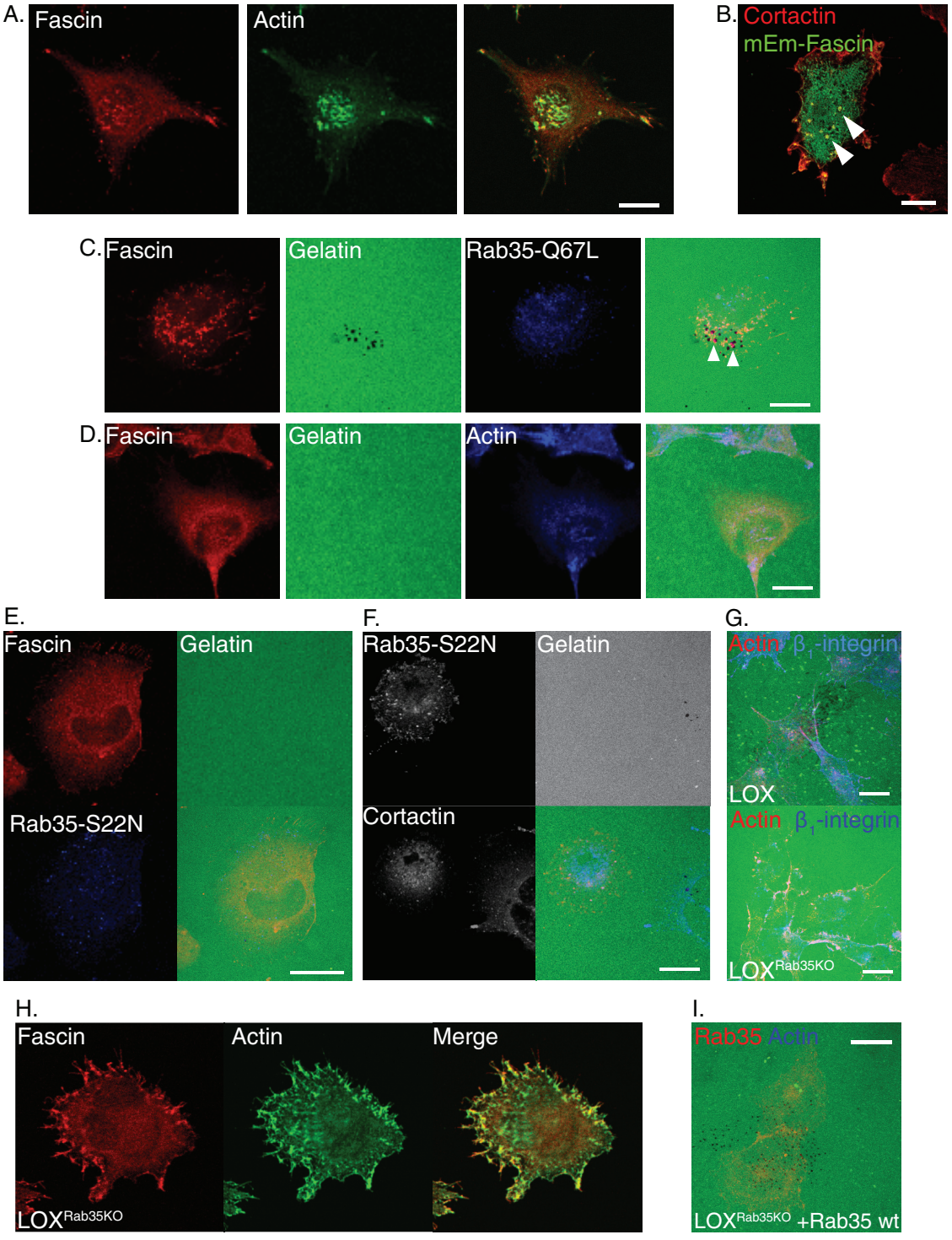

FIG 5 Loss of Rab35 alters intracellular fascin localization. (A) Parental LOX cells plated on unlabeled gelatin were fixed, stained, and analyzed by confocal microscopy to examine the localization of endogenous fascin at the invasive, ventral surfaces of the cells. (B) Fascin localization and cortactin localization were examined together in cells transiently expressing mEmerald-fascin on unlabeled gelatin. Colocalization of both markers is indicative of localization of both components to invadopodia. (C) Invadopodium-mediated degradation, together with the intracellular distribution of endogenous fascin or cortactin, was examined in mesenchymal LOX cells transfected with myc–Rab35-Q67L. Matrix degradation appears as dark spots on the fluorescent background. (D) LOX cells stably expressing dominant-negative ARF6-T27N were plated in a mesenchymal invasion assay and allowed to degrade matrix overnight before being fixed, stained as indicated, and analyzed by confocal microscopy. (E) Confocal immunofluorescent analysis of fascin distribution and invasive capacity in cells subjected to dominant inhibition of Rab35. (F) LOX cells were transfected with dominant-negative Rab35-S22N and used in an invadopodium invasion assay. Scale bar, 25 μm. (G) LOX and LOX^{Rab35KO} cells were plated in an *in vitro* mesenchymal invasion assay and allowed to degrade matrix overnight before being counterstained for actin and β_1-integrin to define cell boundaries; they were then imaged by confocal microscopy. Depletion of Rab35 blocks invadopodium-mediated matrix

(Continued on next page)

readily adopt an amoeboid morphology (3, 4), which is accompanied by active TMV shedding and cell invasion (6, 11, 40). Without Rab35, this shedding and the resulting matrix degradation are dramatically increased. The specific regulators of mesenchymal/amoeboid toggling remain unknown, though it is highly likely that certain GAPs and GEFs are engaged to drive cellular morphology one way or another, in a manner similar to the recent report showing different Rab35 effector proteins regulating PODXL trafficking in 2D versus 3D cultures of epithelial cells (37). These results, however, implicate additional GTPase signaling, which may act to enhance or weaken those transitional signals, providing an additional level of control over cell invasion. As such, we propose that as migrating and invading tumor cells encounter matrices of various mechanical properties, the innate mechanosensory machinery triggers changes in the stoichiometric balance of Rab35-GTP and ARF6-GTP. These changes, likely coupled to similar shifts between active RhoA and Rac1, underlie the resulting morphological changes and adaptive modes of tumor cell invasion.

The recent identification of Rab35 as an oncoprotein increases interest in the development of Rab35-targeted therapies for the prevention of metastases (28). Noteworthy in this regard is that in ovarian cancer patients with high levels of fascin expression, existing meta-analysis reveals an inverse correlation between overall survival or progression-free survival and Rab35 expression. Wheeler et al. have elegantly described the ability of robust Rab35 activation to transform normal cells *in vitro*, linking this activity to somatic mutations identified in patient samples (28). This same study, however, placed Rab35 downstream of receptor tyrosine kinases (RTKs), in line with its previously identified functions regulating the endomembrane system (28). Many receptor tyrosine kinases undergo ligand-stimulated endocytosis, where they enter the endomembrane system, remaining competent to signal while their trafficking is regulated by, among others, Rab35 and ARF6. The resulting signaling endosomes may represent a crucial node through which Rab35 and ARF6 mutually antagonize one another. For example, in breast cancer epidermal growth factor receptor activation results in the GEF-mediated activation of ARF6, leading to adherens junction breakdown and the promotion of an invasive phenotype. Furthermore, in multiple tumor types, including high-grade breast cancers, activation of ARF6 was previously linked to the loss of Rab35 mRNA and the adoption of highly motile and invasive characteristics, which are themselves hallmarks of malignancy (27). These reports, coupled with our results, suggest context-dependent implications for modulations in Rab35 signaling where prolonged RTK signaling first promotes Rab35 activity before it is antagonized by subsequent ARF6 activation, perhaps during the metastatic cascade where the downregulation of Rab35 is directly linked to ARF6-driven proinvasive activities.

Recently, differential expression levels and localization between parental and highly metastatic colorectal cancer cells were reported for Rab35 (41). In highly metastatic cells, Mendes et al. reported a shift to a predominantly peripheral localization for Rab35. Our studies suggest that peripheral Rab35, together with ezrin, would readily be available to interact with and facilitate the recruitment of fascin. The results presented above outline an important mechanism through which depletion of a novel oncoprotein uncouples and unleashes distinct protumorigenic processes. Furthermore, the increased cell invasion seen upon Rab35 depletion indicates that the complex network of Rab35 effectors warrants the development of targeted combinatorial therapies to prevent the formation of a prometastatic condition.

MATERIALS AND METHODS

Antibodies and reagents. Fascin, β_1-integrin, and tubulin antibodies were from Millipore Sigma. Antibodies to myc tag, actin, ERK, p-ERK, ezrin, p-ezrin, Rab35, pAKT, hemagglutinin (HA) tag, and GAPDH

FIG 5 Legend (Continued)
degradation, which appears as dark spots in the control image. (H) Immunofluorescent staining of endogenous fascin at the invasive surface revealed that the intracellular distribution associated with invadopodium formation is lost with depletion of Rab35 and that fascin has a predominantly peripheral localization. (I) Expression of wild-type Rab35 rescues invadopodium-mediated invasive capacity in LOX^{Rab35KO} cells. Unless otherwise indicated, scale bars indicate 20 μm.

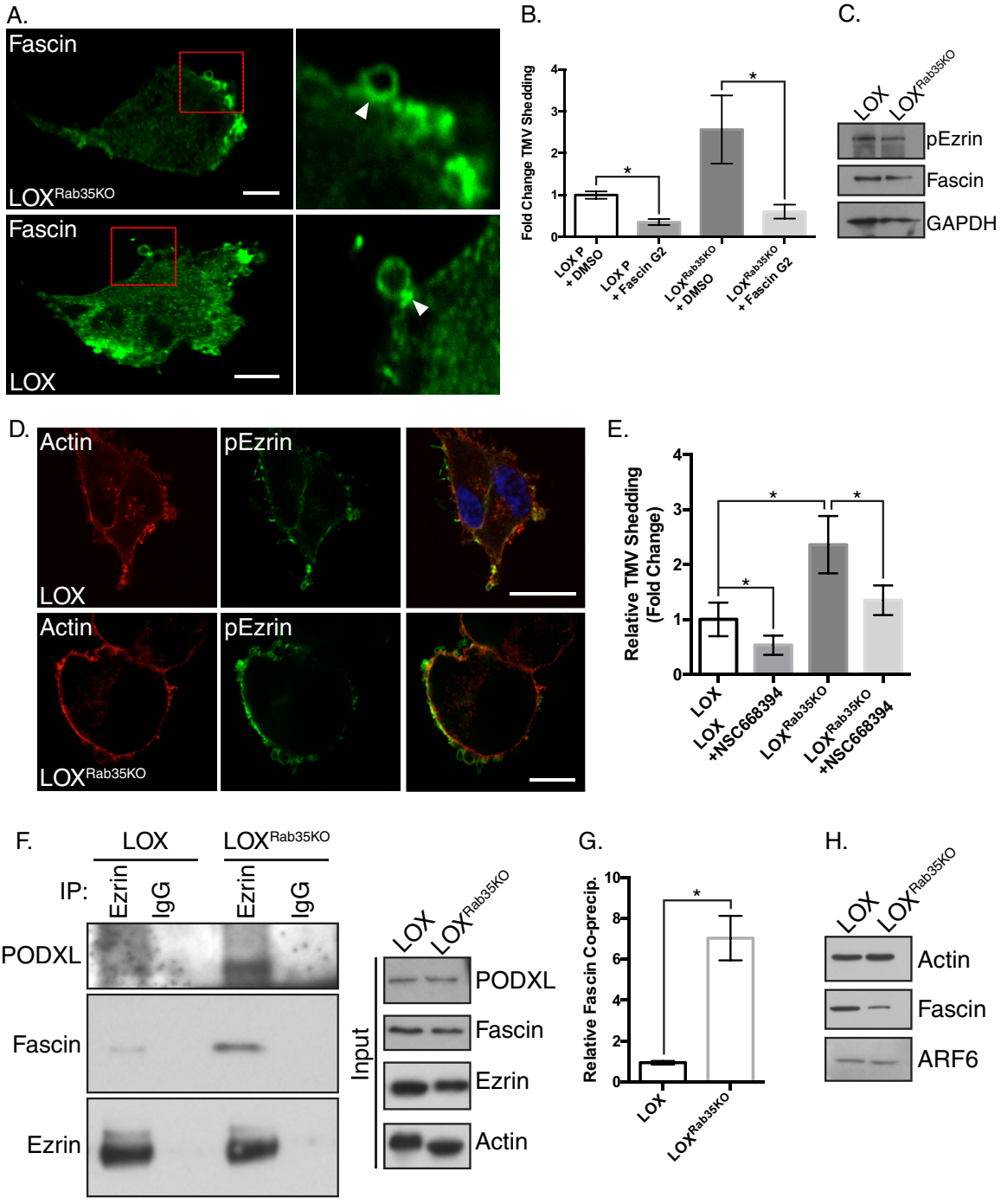

FIG 6 Fascin interacts with peripheral binding partners to facilitate TMV release. (A) Endogenous fascin localization away from the ventral surface, as examined in LOX and LOX^{Rab35KO} cells by immunofluorescence. Fascin can be localized to the necks of budding TMVs in both cell types. (B) Conditioned media from cells treated with vehicle control or the small molecule inhibitor of fascin's actin bundling ability, FascinG2, were analyzed by NTA. Data are presented as means ± the SD (**, $P < 0.02$). (C) Lysates from LOX and LOX^{Rab35KO} cells were separated by SDS-PAGE and analyzed as indicated by Western blotting. (D) Phospho-ezrin distribution was examined in LOX and LOX^{Rab35KO} cells by immunofluorescence. Scale bars, 25 μm (LOX) and 10 μm (LOX^{Rab35KO} cells). (E) TMV concentrations in conditioned media from cells treated with vehicle control or the small molecule inhibitor of ezrin, NSC668394, were analyzed by NTA. Inhibition of ezrin activity reduces TMV shedding upon Rab35 depletion. Data are presented as means ± the SEM (*, $P < 0.001$). (F) Endogenous ezrin was immunoprecipitated from LOX or LOX^{Rab35KO} cells, and the precipitated proteins were separated by SDS-PAGE and examined by Western blotting. (G) Upon loss of Rab35, increased amounts of podocalyxin and fascin coprecipitate with ezrin. Data are presented as means ± the SD (*, $P = 0.012$). (H) TMVs were isolated from LOX and LOX^{Rab35KO} cells, and particle concentrations were determined by NTA. Equal numbers of vesicles were then lysed and examined by Western blotting. Loss of Rab35 leads to a change in the amount of fascin cargo per vesicle.

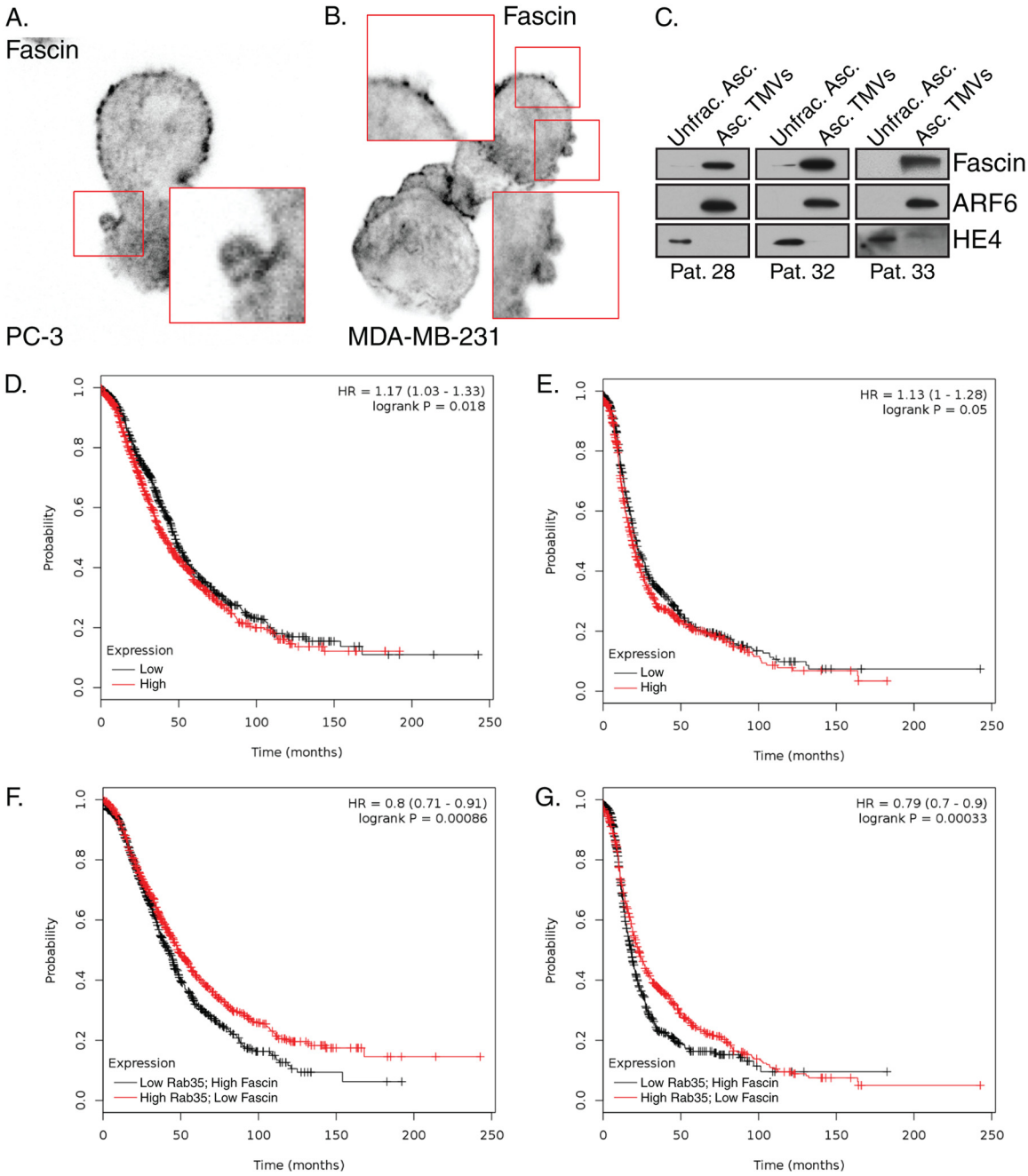

FIG 7 Fascin distribution affects TMV shedding and clinical outcomes. (A and B) Endogenous fascin localization was determined in prostate cancer cells (A) and breast (B) tumor cell lines during amoeboid cell invasion. (C) Equal amounts of protein (determined using a BCA assay) from unfractionated ovarian ascites fluid and purified TMVs from patient samples were separated by SDS-PAGE and probed for fascin, ARF6, or HE4 content by Western blotting. Note that the protein is equal within but not between patients. Representative data are shown from patients later diagnosed with serous cystadenocarcinoma of the ovary (29), high-grade serous ovarian carcinoma (33), and poorly differentiated ovarian carcinoma (34). (D and E) Overall survival (D) and progression-free survival (E) were compared in patient cohorts (n = 1,657 and n = 1,436, respectively) with high or low fascin expression based on the various quantile expression levels; the two patient cohorts are compared by a Kaplan-Meier survival plot, with the hazard ratio, 95% confidence intervals, and log-rank P value calculated as previously reported (49, 50). (F and G) Overall (F) and progression-free (G) survival measures were also calculated using similar techniques for high fascin values coupled to low Rab35 expression levels.

(glyceraldehyde-3-phosphate dehydrogenase) were from Cell Signaling. Antibody to human PODXL was obtained from BioTechne, and antibodies to ARF6 were as described previously (42). Fluorophore-conjugated secondary antibodies were from Jackson Immuno; horseradish peroxidase-conjugated secondary antibodies were from Cell Signaling. U-0126, ML-7, NSC27632, and NSC668394 were purchased from EMD-Millipore, and FascinG2 was obtained from XcessBio.

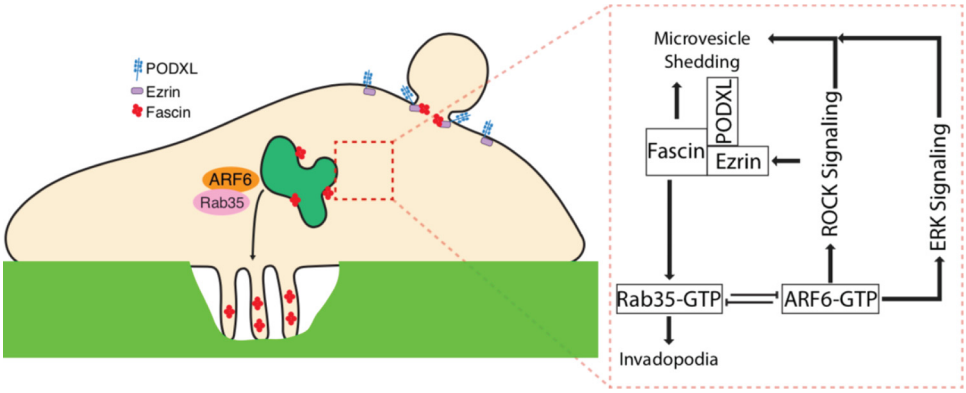

FIG 8 Working model outlines Rab35-ARF6-regulated TMV shedding. Working model for the intracellular signaling pathways governing the Rab35- and ARF6-regulated trafficking of fascin to distinct invasive structures. Rab35 inactivation blocks fascin recruitment to invadopodia from endomembrane structures. Instead, peripheral fascin is trapped at sites of TMV shedding, where it is bound in a complex with ezrin and PODXL and readily available to facilitate amoeboid cell invasion.

Cell culture, transfection, and Rab35 knockdown. The LOX cell line (provided by Oystein Fodstad, Oslo University) was maintained as previously described (13). A375-MA2, A357P, OvCar3, and MDA-MB-231 cell lines were purchased from ATCC and maintained according to ATCC guidelines. PC-3 cells were cultured in F-12K (Gibco) supplemented with 10% serum, 2 mM L-glutamine, and penicillin-streptomycin mix. Cultures were maintained at 37°C and 5% CO_2 in a humidified incubator. Rab35 mutant plasmids were generated by subcloning of myc-tagged Rab35 constructs from pBI-EGFP (kindly provided by Guangpu Li) into a pLNCX-2 background. pSpCas9(BB)-2A-GFP (PX458) and lentiCRISPR v2 were gifts from Feng Zhang (43, 44). Guide RNA targeting Rab35 was inserted into the CRISPR backbones as previously described (45, 46). Plasmids were transfected into target cells using Lipofectamine 2000. To generate the clonal line, cells were passed through limiting dilution of 0.8 cells/well into 96-well plates. Potential clones were screened for knockdown of Rab35 by Western blotting. Lentivirus-mediated knockdown was carried out as described previously (44, 46). At 72 h after infection, puromycin was added to the culture media at a final concentration of 0.25 μg/ml for 7 days, resulting in a nonclonal heterogeneous population enriched for knockdown cells.

Immunoprecipitations and Western blotting. Cells were lysed in buffer containing 150 mM NaCl, 1 mM EDTA, 1 mM EGTA, 20 mM Tris-HCl (pH 7.5), and 1% Triton X-100 with fresh mammalian protease inhibitor (MPI) cocktail (Millipore Sigma) for Western blotting experiments. Triton insoluble fractions were removed by centrifugation at 15,000 $\times$ *g* for 15 min. Lysates were then ready for use in downstream applications. For immunoprecipitations, cells were lysed in coimmunoprecipitation buffer containing 20 mM Tris-HCl (pH 8.0), 150 mM NaCl, 20 mM KCl, 1.5 mM $MgCl_2$, 0.5% Triton X-100, and MPI. Insoluble fractions were removed by centrifugation, and lysates were precleared by incubation with Protein A/G Plus-agarose beads (Santa Cruz Biotechnology) for 1 h at 4°C with gentle inversion. Precleared lysates were then incubated with primary antibody overnight at 4°C with gentle inversion. Fresh Protein A/G Plus beads were added to the antibody mix and inverted for 1 h at 4°C. Bead-bound proteins were isolated by centrifugation at 300 $\times$ *g* for 2 min, the supernatant was removed, and 1 ml of fresh lysis buffer was added. This was repeated for a total of three washes. Isolated beads were resuspended in 1$\times$ SDS loading dye, followed by incubation in a boiling water bath for 6 min before separation by SDS-PAGE. PAGE gels were then transferred to a polyvinylidene difluoride membrane (Millipore Sigma). Nonspecific binding was blocked by incubation in 5% nonfat milk in Tris-buffered saline plus 0.05% Tween 20 for 1 h at room temperature. Primary antibody incubation was carried out based on the manufacturer's recommendations.

Microvesicle isolation. TMVs were isolated from cells at ~80% confluence at the time of collection. Conditioned medium was removed, and the cells rinsed once with sterile phosphate-buffered saline (PBS), which was then combined with the collected media. Conditioned medium was then centrifuged for 15 min at 300 $\times$ *g* to remove cells and large debris, and the supernatant was centrifuged for 20 min at 2,000 $\times$ *g*. TMVs were subsequently isolated by centrifugation at 10,000 $\times$ *g* for 30 min. The resulting pellet was washed in sterile PBS two times before a final isolation prior to downstream use.

Nanoparticle tracking analysis. Conditioned media or TMVs were isolated from cells as described above. TMVs were resuspended in filtered PBS and injected into a NanoSight LM10 equipped with a 488-nm laser. Particles were tracked for 90 s, and tracking analysis carried out using NanoSight NTA software as previously described (47, 48). Briefly, particles in suspension scatter a laser beam passing through the sample chamber in such a manner that they can easily be visualized at $\times$20 magnification. The attached camera captures a video file of the particles moving under Brownian motion. The software subsequently tracks many individual particles, estimating their hydrodynamic diameters using the Stokes-Einstein equation.

Immunofluorescence and invasion assays. For immunofluorescence, cells or microvesicles were plated on glass or gelatin-coated coverslips, fixed in ice-cold 100% methanol (for fascin) or 2%

paraformaldehyde, washed three times with 1× PBS, prepermeabilized with 1× PBS plus 0.3% Triton X-100, blocked and permeabilized in 5% bovine serum albumin–0.2% Triton X-100–0.05% Tween 20 in 1× PBS, and incubated with primary antibodies as indicated. The cells were then incubated with fluorophore-conjugated secondary antibodies and mounted using antifade gold mounting media. Invasion assays were carried out as previously described (6, 11). Briefly, cells were trypsinized, and a single cell suspension was overlaid onto coverslips coated with FITC-conjugated matrix, which allows the visualization of invasion/matrix degradation as dark spots or trails on a fluorescent background. Immunofluorescence images on fixed cells were acquired using either a Nikon A1R confocal microscope or a Bio-Rad 1024 MRC confocal microscope.

Patient samples. Ascites or intraperitoneal saline washings (when ascites was not present) were collected from patients giving informed consent according to the protocol approved by the university's Human Subjects Institutional Review Board (HSIRB) and the Northern Indiana Cancer Research Consortium Institutional Review Board. TMVs were isolated as indicated above.

ACKNOWLEDGMENTS

This study was supported in part by grants from the National Cancer Institute (R01CA115316) and the Catherine Peachey Foundation to C.D.-S.

We also gratefully acknowledge Michael Method and the staff at Michiana Hematology Oncology for their assistance with acquisition of clinical samples, and we thank Guangpu Li for the Rab35 plasmids. We declare no competing conflicts of interest.

Author contributions to article were as follows: conceptualization, C.D.-S. and J.W.C.; methodology, J.W.C. and C.D.-S.; investigation, J.W.C., C.J.T., and D.R.M.; writing (original draft), J.W.C. and C.D.-S.; writing (review and editing), J.W.C., C.J.T., D.R.M., and C.D.-S.; supervision, C.D.-S. and J.W.C.; and funding, C.D.-S.

REFERENCES

1. Orgaz JL, Pandya P, Dalmeida R, Karagiannis P, Sanchez-Laorden B, Viros A, Albrengues J, Nestle FO, Ridley AJ, Gaggioli C, Marais R, Karagiannis SN, Sanz-Moreno V. 2014. Diverse matrix metalloproteinase functions regulate cancer amoeboid migration. Nat Commun 5:4255. https://doi.org/10.1038/ncomms5255.
2. Te Boekhorst V, Preziosi L, Friedl P. 2016. Plasticity of cell migration *in vivo* and *in silico*. Annu Rev Cell Dev Biol 32:491–526. https://doi.org/10.1146/annurev-cellbio-111315-125201.
3. Sahai E, Marshall CJ. 2003. Differing modes of tumour cell invasion have distinct requirements for Rho/ROCK signalling and extracellular proteolysis. Nat Cell Biol 5:711–719. https://doi.org/10.1038/ncb1019.
4. Sanz-Moreno V, Gadea G, Ahn J, Paterson H, Marra P, Pinner S, Sahai E, Marshall CJ. 2008. Rac activation and inactivation control plasticity of tumor cell movement. Cell 135:510–523. https://doi.org/10.1016/j.cell.2008.09.043.
5. Lammermann T, Sixt M. 2009. Mechanical modes of 'amoeboid' cell migration. Curr Opin Cell Biol 21:636–644. https://doi.org/10.1016/j.ceb.2009.05.003.
6. Sedgwick AE, Clancy JW, Olivia Balmert M, D'Souza-Schorey C. 2015. Extracellular microvesicles and invadopodia mediate non-overlapping modes of tumor cell invasion. Sci Rep 5:14748. https://doi.org/10.1038/srep14748.
7. Peinado H, Aleckovic M, Lavotshkin S, Matei I, Costa-Silva B, Moreno-Bueno G, Hergueta-Redondo M, Williams C, Garcia-Santos G, Ghajar C, Nitadori-Hoshino A, Hoffman C, Badal K, Garcia BA, Callahan MK, Yuan J, Martins VR, Skog J, Kaplan RN, Brady MS, Wolchok JD, Chapman PB, Kang Y, Bromberg J, Lyden D. 2012. Melanoma exosomes educate bone marrow progenitor cells toward a pro-metastatic phenotype through MET. Nat Med 18:883–891. https://doi.org/10.1038/nm.2753.
8. Abels ER, Breakefield XO. 2016. Introduction to extracellular vesicles: biogenesis, RNA cargo selection, content, release, and uptake. Cell Mol Neurobiol 36:301–312. https://doi.org/10.1007/s10571-016-0366-z.
9. Desrochers LM, Antonyak MA, Cerione RA. 2016. Extracellular vesicles: satellites of information transfer in cancer and stem cell biology. Dev Cell 37:301–309. https://doi.org/10.1016/j.devcel.2016.04.019.
10. Kim J, Morley S, Le M, Bedoret D, Umetsu DT, Di Vizio D, Freeman MR. 2014. Enhanced shedding of extracellular vesicles from amoeboid prostate cancer cells: potential effects on the tumor microenvironment. Cancer Biol Ther 15:409–418. https://doi.org/10.4161/cbt.27627.
11. Clancy JW, Sedgwick A, Rosse C, Muralidharan-Chari V, Raposo G, Method M, Chavrier P, D'Souza-Schorey C. 2015. Regulated delivery of molecular cargo to invasive tumour-derived microvesicles. Nat Commun 6:6919. https://doi.org/10.1038/ncomms7919.
12. Hoshino D, Kirkbride KC, Costello K, Clark ES, Sinha S, Grega-Larson N, Tyska MJ, Weaver AM. 2013. Exosome secretion is enhanced by invadopodia and drives invasive behavior. Cell Rep 5:1159–1168. https://doi.org/10.1016/j.celrep.2013.10.050.
13. Muralidharan-Chari V, Clancy J, Plou C, Romao M, Chavrier P, Raposo G, D'souza-Schorey C. 2009. ARF6-regulated shedding of tumor cell-derived plasma membrane microvesicles. Curr Biol 19:1875–1885. https://doi.org/10.1016/j.cub.2009.09.059.
14. Tricarico C, Clancy J, D'Souza-Schorey C. 2016. Biology and biogenesis of shed microvesicles. Small GTPases 8:220–232. https://doi.org/10.1080/21541248.2016.1215283.
15. D'Souza-Schorey C, Chavrier P. 2006. ARF proteins: roles in membrane traffic and beyond. Nat Rev Mol Cell Biol 7:347–358. https://doi.org/10.1038/nrm1910.
16. Zhang J, Fonovic M, Suyama K, Bogyo M, Scott MP. 2009. Rab35 controls actin bundling by recruiting fascin as an effector protein. Science 325:1250–1254. https://doi.org/10.1126/science.1174921.
17. Chaineau M, Ioannou MS, McPherson PS. 2013. Rab35: GEFs, GAPs, and effectors. Traffic 14:1109–1117. https://doi.org/10.1111/tra.12096.
18. Klinkert K, Echard A. 2016. Rab35 GTPase: a central regulator of phosphoinositides and F-actin in endocytic recycling and beyond. Traffic 17:1063–1077. https://doi.org/10.1111/tra.12422.
19. Hanono A, Garbett D, Reczek D, Chambers DN, Bretscher A. 2006. EPI64 regulates microvillar subdomains and structure. J Cell Physiol 175:803–813. https://doi.org/10.1083/jcb.200604046.
20. Kobayashi H, Fukuda M. 2012. Rab35 regulates Arf6 activity through centaurin-β2 (ACAP2) during neurite outgrowth. J Cell Sci 125:2235–2243. https://doi.org/10.1242/jcs.098657.
21. Rahajeng J, Giridharan SS, Cai B, Naslavsky N, Caplan S. 2012. MICAL-L1 is a tubular endosomal membrane hub that connects Rab35 and Arf6 with Rab8a. Traffic 13:82–93. https://doi.org/10.1111/j.1600-0854.2011.01294.x.
22. Miyamoto Y, Yamamori N, Torii T, Tanoue A, Yamauchi J. 2014. Rab35, acting through ACAP2 switching off Arf6, negatively regulates oligodendrocyte differentiation and myelination. Mol Biol Cell 25:1532–1542. https://doi.org/10.1091/mbc.E13-10-0600.
23. Dutta D, Donaldson JG. 2015. Sorting of clathrin-independent cargo proteins depends on Rab35 delivered by clathrin-mediated endocytosis. Traffic 16:994–1009. https://doi.org/10.1111/tra.12302.
24. Chen L, Yang S, Jakoncic J, Zhang JJ, Huang XY. 2010. Migrastatin

analogues target fascin to block tumour metastasis. Nature 464:1062–1066. https://doi.org/10.1038/nature08978.
25. Sabeh F, Shimizu-Hirota R, Weiss SJ. 2009. Protease-dependent versus -independent cancer cell invasion programs: three-dimensional amoeboid movement revisited. J Cell Physiol 185:11–19. https://doi.org/10.1083/jcb.200807195.
26. Wolf K, Te Lindert M, Krause M, Alexander S, Te Riet J, Willis AL, Hoffman RM, Figdor CG, Weiss SJ, Friedl P. 2013. Physical limits of cell migration: control by ECM space and nuclear deformation and tuning by proteolysis and traction force. J Cell Biol 201:1069–1084. https://doi.org/10.1083/jcb.201210152.
27. Allaire PD, Seyed Sadr M, Chaineau M, Seyed Sadr E, Konefal S, Fotouhi M, Maret D, Ritter B, Del Maestro RF, McPherson PS. 2013. Interplay between Rab35 and Arf6 controls cargo recycling to coordinate cell adhesion and migration. J Cell Sci 126:722–731. https://doi.org/10.1242/jcs.112375.
28. Wheeler DB, Zoncu R, Root DE, Sabatini DM, Sawyers CL. 2015. Identification of an oncogenic RAB protein. Science 350:211–217. https://doi.org/10.1126/science.aaa4903.
29. Tague S, Muralidharan V, D'Souza-Schorey C. 2004. ADP-ribosylation factor 6 regulates tumor cell invasion through the activation of the MEK/ERK signaling pathway. Proc Natl Acad Sci U S A 101:9671. https://doi.org/10.1073/pnas.0403531101.
30. Muralidharan-Chari V, Hoover H, Clancy J, Schweitzer J, Suckow MA, Schroeder V, Castellino FJ, Schorey JS, D'souza-Schorey C. 2009. ADP-ribosylation factor 6 regulates tumorigenic and invasive properties *in vivo*. Cancer Res 69:2201–2209. https://doi.org/10.1158/0008-5472.CAN-08-1301.
31. Murphy DA, Courtneidge SA. 2011. The 'ins' and 'outs' of podosomes and invadopodia: characteristics, formation and function. Nat Rev Mol Cell Biol 12:413–426. https://doi.org/10.1038/nrm3141.
32. Li A, Dawson JC, Forero-Vargas M, Spence HJ, Yu X, Konig I, Anderson K, Machesky LM. 2010. The actin-bundling protein fascin stabilizes actin in invadopodia and potentiates protrusive invasion. Curr Biol 20:339–345. https://doi.org/10.1016/j.cub.2009.12.035.
33. Huang FK, Han S, Xing B, Huang J, Liu B, Bordeleau F, Reinhart-King CA, Zhang JJ, Huang XY. 2015. Targeted inhibition of fascin function blocks tumour invasion and metastatic colonization. Nat Commun 6:7465. https://doi.org/10.1038/ncomms8465.
34. Tran Quang C, Gautreau A, Arpin M, Treisman R. 2000. Ezrin function is required for ROCK-mediated fibroblast transformation by the Net and Dbl oncogenes. EMBO J 19:4565–4576. https://doi.org/10.1093/emboj/19.17.4565.
35. Chen Y, Wang D, Guo Z, Zhao J, Wu B, Deng H, Zhou T, Xiang H, Gao F, Yu X, Liao J, Ward T, Xia P, Emenari C, Ding X, Thompson W, Ma K, Zhu J, Aikhionbare F, Dou K, Cheng SY, Yao X. 2011. Rho kinase phosphorylation promotes ezrin-mediated metastasis in hepatocellular carcinoma. Cancer Res 71:1721–1729. https://doi.org/10.1158/0008-5472.CAN-09-4683.
36. Sizemore S, Cicek M, Sizemore N, Ng KP, Casey G. 2007. Podocalyxin increases the aggressive phenotype of breast and prostate cancer cells *in vitro* through its interaction with ezrin. Cancer Res 67:6183–6191. https://doi.org/10.1158/0008-5472.CAN-06-3575.
37. Mrozowska PS, Fukuda M. 2016. Regulation of podocalyxin trafficking by Rab small GTPases in 2D and 3D epithelial cell cultures. J Cell Biol 213:355–369. https://doi.org/10.1083/jcb.201512024.
38. Tan VY, Lewis SJ, Adams JC, Martin RM. 2013. Association of fascin-1 with mortality, disease progression and metastasis in carcinomas: a systematic review and meta-analysis. BMC Med 11:52. https://doi.org/10.1186/1741-7015-11-52.
39. Bulut G, Hong SH, Chen K, Beauchamp EM, Rahim S, Kosturko GW, Glasgow E, Dakshanamurthy S, Lee HS, Daar I, Toretsky JA, Khanna C, Uren A. 2012. Small molecule inhibitors of ezrin inhibit the invasive phenotype of osteosarcoma cells. Oncogene 31:269–281. https://doi.org/10.1038/onc.2011.245.
40. Di Vizio D, Kim J, Hager MH, Morello M, Yang W, Lafargue CJ, True LD, Rubin MA, Adam RM, Beroukhim R, Demichelis F, Freeman MR. 2009. Oncosome formation in prostate cancer: association with a region of frequent chromosomal deletion in metastatic disease. Cancer Res 69:5601–5609. https://doi.org/10.1158/0008-5472.CAN-08-3860.
41. Mendes M, Pelaez-Garcia A, Lopez-Lucendo M, Bartolome RA, Calvino E, Barderas R, Casal JI. 2017. Mapping the spatial proteome of metastatic cells in colorectal cancer. Proteomics 17:1700094. https://doi.org/10.1002/pmic.201700094.
42. Schweitzer JK, D'Souza-Schorey C. 2002. Localization and activation of the ARF6 GTPase during cleavage furrow ingression and cytokinesis. J Biol Chem 277:27210–27216. https://doi.org/10.1074/jbc.M201569200.
43. Ran FA, Hsu PD, Wright J, Agarwala V, Scott DA, Zhang F. 2013. Genome engineering using the CRISPR-Cas9 system. Nat Protoc 8:2281–2308. https://doi.org/10.1038/nprot.2013.143.
44. Sanjana NE, Shalem O, Zhang F. 2014. Improved vectors and genome-wide libraries for CRISPR screening. Nat Methods 11:783–784. https://doi.org/10.1038/nmeth.3047.
45. Cong L, Ran FA, Cox D, Lin S, Barretto R, Habib N, Hsu PD, Wu X, Jiang W, Marraffini LA, Zhang F. 2013. Multiplex genome engineering using CRISPR/Cas systems. Science 339:819–823. https://doi.org/10.1126/science.1231143.
46. Shalem O, Sanjana NE, Hartenian E, Shi X, Scott DA, Mikkelson T, Heckl D, Ebert BL, Root DE, Doench JG, Zhang F. 2014. Genome-scale CRISPR-Cas9 knockout screening in human cells. Science 343:84–87. https://doi.org/10.1126/science.1247005.
47. Filipe V, Hawe A, Jiskoot W. 2010. Critical evaluation of nanoparticle tracking analysis (NTA) by NanoSight for the measurement of nanoparticles and protein aggregates. Pharm Res 27:796–810. https://doi.org/10.1007/s11095-010-0073-2.
48. Malloy A. 2011. Count, size, and visualize nanoparticles. Materials Today 14:170–173. https://doi.org/10.1016/S1369-7021(11)70089-X.
49. Gyorffy B, Lanczky A, Szallasi Z. 2012. Implementing an online tool for genome-wide validation of survival-associated biomarkers in ovarian-cancer using microarray data from 1287 patients. Endocr Relat Cancer 19:197–208. https://doi.org/10.1530/ERC-11-0329.
50. Lánczky A, Nagy Á, Bottai G, Munkácsy G, Szabó A, Santarpia L, Győrffy B. 2016. miRpower: a web-tool to validate survival-associated miRNAs utilizing expression data from 2178 breast cancer patients. Breast Cancer Res Treat 160:439–446. https://doi.org/10.1007/s10549-016-4013-7.